INDIAN JOURNAL OF SCIENCE AND TECHNOLOGY

RESEARCH ARTICLE

Green synthesis of Ceriumoxide Nanoparticles using *Bacopa monnieri* Leaf Extract - *In vitro A* ntioxidant Activity

Mamatha Madhugiri Gopinath[1], Sumreen Sultana[1], Shital Manohar Punekar[1], M B Nivedika[1], Ravikiran Tekupalli[1]*

1 Department of Microbiology and Biotechnology, Bangalore University, Bengaluru, 560056, India

OPEN ACCESS

Received: 28-11-2022

Accepted: 17-01-2023

Published: 09-03-2023

Citation: Gopinath MM, Sultana S, Punekar SM, Nivedika MB, Tekupalli R (2023) Green synthesis of Ceriumoxide Nanoparticles using *Bacopa monnieri* Leaf Extract - *In vitro A* ntioxidant Activity. Indian Journal of Science and Technology 16(10): 698-706. https://doi.org/10.17485/IJST/v16i10.2291

* **Corresponding author**.

ravikiran@bub.ernet.in

Funding: None

Competing Interests: None

Published By Indian Society for Education and Environment (iSee)

ISSN
Print: 0974-6846
Electronic: 0974-5645

Abstract

Objectives: Cerium oxide nanoparticles were synthesized by a rapid green method using an aqueous leaf extract of *Bacopa monnieri* to investigate its antioxidant activity. **Methods**: Cerium oxide nanoparticles (CeO_2 NPs) were synthesized using *Bacopa monnieri* leaf extract as a stabilizing agent by solution combustion method. Characterization techniques like FTIR, PXRD,SEM-EDAX, HR-TEM, UV-visible, and Raman spectroscopy confirmed the synthesized NPs. The antioxidant capacity was assessed by *in vitro* Hydroxyl radical scavenging assay. **Findings**: The biosynthesized CeO_2 NPs possess tiny spherical shapes and sizes ranging from 5-50nm, and the average particle size is 27 nm as measured by HR-TEM. XRD and Raman confirm the nanoparticle's polycrystalline nature and face-centered cubic fluorite structure with maximum UV-visible absorbance at λ_{max} 301.2nm. The biosynthesized CeO_2 NPs exhibited better scavenging activity than Vitamin C. However, further *in vitro* and *in vivo* studies must be warranted to explore its mechanism and therapeutic potential. **Novelty:** To the best of our knowledge, this is the first report involving the green synthesis of cerium oxide nanoparticles using *Bacopa monnieri* leaf extract, which exhibited potent hydroxyl radical scavenging activity which can be a promising therapeutic candidate in oxidative stress-related disorders.

Keywords: CeO2 NPs; Green synthesis; Bacopa monnieri; HR-TEM; Hydroxyl radical

1 Introduction

Nanotechnology deals with nanoparticles (NPs) that are atomic or molecular aggregates characterized by a size of less than 100 nm and are key players in modern medicine with applications ranging from bioimaging to therapeutic drugs [(1)]. Among various inorganic NPs, CeO_2 NPs have received much attention due to their practical applications as catalysts, chemical polishing, fuel cells, and antioxidants in biological systems [(2)].

Recently, cerium oxide nanoparticles possessing anti-oxidative properties have emerged as potential therapeutic agents in various fields including nanomedicine [(3)].

Cerium is a member of the lanthanide series with a fluorite structure and rare earth oxide material, as it is most abundant in the earth's crust, among other elements [4]. It also possesses a unique electronic configuration due to the large surface area to volume ratio that creates oxygen defects on its surface [5]. Many unique features are mainly linked with the co-existence of a dual oxidation Ce^{4+} and Ce^{3+} state at the nanoparticle surface, enabling them to act as oxidizing and reducing agents [6]. Recent studies reported CeO_2 NPs mimetic superoxide dismutase and catalase activity and have emerged as a fascinating material in biological fields [7].

Typically, nanoparticles are synthesized from various chemical and physical methods, which are costly, inefficient, and energy-intensive, and also utilize toxic chemicals that lead to hazardous waste production in the environment [8,9]. Nowadays, scientists are adapting the principles of green chemistry for the synthesis of nanoparticles as they are safe and non-toxic [10]. Plants are considered as the most potential agent for the green synthesis due to their easy availability, safe and ecofriendly nature. Plants are rich source of secondary metabolites such as polyphenols, alkaloids, flavonoids, and terpenoids which act as stabilizing and capping agents [11].

Plant-mediated nanoparticle synthesis is considered eco-friendly, biocompatible, and possesses a wide variety of secondary metabolites [12]. Different plant extracts have been used for the synthesis of CeO_2 NPs, including *Origanum majorana. L* [13], *Ceratonia silique. L* [14], *Moringa oleifera* [15], *Jatropha curcus* [16], and *Acorus calamus* [17]. The phytochemicals wrap effectively on NP's surface, thus showing higher catalytic reactivity and greater surface area, which play an essential role in adsorbing and neutralizing free radicals [18]. Indian traditional medicine uses various herbs to treat several diseases. One such medicinal plant is *Bacopa monnieri* (*B. monnieri*), which belongs to Plantiginaceae. It is commonly known as Bramhi or Medha rasayanas and is used in Ayurveda as a memory enhancer, analgesic, anti-inflammatory, antiepileptic, antidiarrhoeal, anticancer, and sedative agent [19]. It contains alkaloids, flavonoids, glycosides, and distinctive saponins called "bacosides" [20].

Numerous studies have reported that green synthesized CeO_2 NPs exhibits varying antioxidant activity. The studies of Yulizar et al., [21] showed that CeO_2 NPs synthesized by *Datura metel L.* leaf extract exhibited considerable free radical scavenging activity (16.61%). Whereas, green synthesized CeO_2 NPs from different plant extract reported the highest antioxidant activity at 500μg/mL [22,23]. Therefore, the present study aimed to biosynthesize CeO_2 NPs, using *B. monnieri* leaf extract as a reducing agent, and to evaluate its antioxidant activity.

2 Methodology

2.1 Chemicals and reagents

Cerium nitrate hexahydrate ($Ce(NO_3)_3.6H_2O$), Deoxy-2-ribose, and Thiobarbituric acid were obtained from Sigma (St. Louis, MO, USA). All organic solvents were of spectral grade, and general chemicals were of analytical quality and were purchased from local companies.

2.2 Collection of plant material

The leaves of *B. monnieri* were collected from local market in Bangalore. The authentication of plant material (RRCBI-19971) was done in the department of Botany, Central Ayurveda Research Institute, Bangalore.

2.3 Preparation of plant extracts

The fresh leaves of *B. monnieri* were washed thoroughly under running tap water and shade dried at room temperature. The dried leaves were finely powdered using a blender. The aqueous leaf extract was prepared following the procedure [24]. Briefly, the powdered samples were soaked in distilled water for about 24hrs. The extract was filtered through Whatman filter paper no-1, and the filtrate was collected, lyophilized and stored at -20 °C until further use.

2.4 Biochemical assays of aqueous leaf extract

2.4.1 Determination of phenol content

The phenol content was determined in the extract using the method [25]. Appropriate extract dilutions were mixed with 2.5 mL of 10 % Folin-Ciocalteau's regent (v/v) and neutralized with 2.0 mL of 7.5 % sodium carbonate. The reaction mixture was incubated for 40 min at 45 °C, and the absorbance was measured at 765 nm in the spectrophotometer. The total phenol content was calculated using gallic acid as standard.

2.4.2 Determination of flavonoid content

The flavonoid content of the extract was determined according to the method [26]. Briefly, 0.5 mL of appropriately diluted sample was mixed with 0.5 ml methanol, 50 μL of 10 % $AlCl_3$, 50μL of 1 M Potassium acetate, and 1.4 ml water and incubated at RT for 30 minutes. After that, the absorbance of the reaction mixture was measured at 415 nm. The total flavonoids were calculated using quercetin as standard.

2.5 Synthesis of CeO2 NPs

The CeO_2 NPs were synthesized by solution combustion according to the protocol [27]. Initially, 0.5g of lyophilized *B. monnieri* aqueous extract was added to 50 ml distilled water and continuously stirred. Then 30ml of aqueous leaf extract was mixed with 0.5g of precursor $Ce(NO_3)_3.6H_2O$ (99.99% pure, 0.036M, pH 3.7) on a magnetic stirrer. Later, the reaction mixture was poured in to porcelain crucible and placed in the pre-heated muffle furnace at 572$\pm$20 ^oC until nanoparticle formation (around 30min).

2.6 Characterization of CeO2 NPs

2.6.1 Fourier Transform Infrared (FTIR spectroscopy)

The Fourier transform Infrared (FTIR) spectra of the standard and green synthesized CeO_2 NPs were recorded on FTIR Perkin Elmer Spectrometer (Spectrum 1000) By KBr pellet method in the scanning range of 400-4000 cm^{-1} at 4 cm^{-1} resolution.

2.6.2 X-ray diffraction (XRD measurement)

X-ray diffractograms of synthesized CeO_2 NPs were obtained with an X-ray diffractometer (Smartlab, Rigaku) using Ni-filtered CuKα radiation (1.2kW, 40kV, 30mA).

2.6.3 Scanning Electron Microscopy (SEM)

The surface morphology of the green synthesized CeO_2 NPs was characterized by a scanning electron microscope (TM 3000, Hitachi, Japan). The powdered CeO_2 NP sample was sprinkled on an aluminum stub using double-sided carbon tape. The image was captured in SEM mode at desired magnification.

2.6.4 High resolution-Transmission Electron Microscopy (HR-TEM)

HR-TEM analysis of the green synthesized CeO_2 NPs was carried out by Tecnai G2, F30 FEI, with an accelerating voltage of up to 300 kV and a Spot resolution of 2.0 Å.

2.6.5 UV- Vis spectral analysis

The UV–Vis analysis was performed using a UV-Vis spectrophotometer (Multiscan GO, Thermo Scientific) and scanning the spectra between 200 and 800 nm at the resolution of 1 nm.

2.6.6 Raman spectroscopy

The synthesized CeO_2 NPs were analyzed using Raman spectroscopy (ID Raman reader) to obtain vibrational modes information. The wavelength of laser light was set at 785 nm and scanned at 200 to 2,000 cm^{-1}.

2.7 Free radical scavenging activity

2.7.1 Hydroxyl radical assay

Hydroxyl radical scavenging assay was determined according to the method [28]. Briefly, different concentrations of the sample (0.195-50μl) were added to a reaction mixture containing 120μL of 20mM deoxyribose, 400μL of 0.1M phosphate buffer, 40μL of 20mM H_2O_2, 40μL of 500mM $FeSO_4$, and the final volume was made up to 800μL with distilled water. The reaction mixture was incubated at 37 °C for 30min. After the incubation period, 0.5mL of 2.8% TCA was added to stop the reaction, followed by the addition of 0.4mL of 0.6% TBA solution. The reaction mixtures were subsequently incubated in a boiling water bath for 20min. The absorbance was measured at 532 nm in a spectrophotometer.

$$Scavenging\ effect\ (\%) = \frac{Absorbance\ (control) - Absorbance\ (sample)}{Absorbance\ (control)} \times 100 \quad (1)$$

Where, Absorbance (control) = absorbance of the control (reacting mixture without the test sample) and Abs (sample) = absorbance of the mixture with the test sample.

Table 1. Total phenol and flavonoid content *B.monnieri* leaves extract

Green synthesized CeO_2 NPs (30 ml extract volume)	
Total phenols (mg GAE/g extract)	Total flavonoids (mg QE/g extract)
110.64±2.15	92.47±1.79

Values are represented as mean ± S.E (n=3)

3 Results and Discussion

In our study, the aqueous leaf extract of *B. monnieri* was used for the green synthesis of CeO_2 NPs. *B. monnieri* is a rich source of secondary metabolites such as phenols and flavonoids, which plays a significant role as reducing and stabilizing agents. These metabolites can act as binding molecules around the cerium atoms (Ce^{3+}), which help form CeO_2 NPs at 570±20 °C. The total Phenol (TPC) and Flavonoid (TFC) content was estimated. The TPC value was found to be 110.64±2.15mg GAE/g extract, and TFC was found to be 92.47±1.79mg QE/g extract, as represented in Table 1 . Our results revealed that phenol content was more than flavonoids which confirms the plausible participation of phenols in the reduction of metal nitrate to metal oxides.

The synthesized NPs were further characterized by FTIR spectroscopy to identify the biomolecules responsible for reducing and stabilizing the cerium oxide nanoparticles. The FTIR spectrum of cerium oxide nanoparticles is shown in Figure 1 a. The spectrum was recorded in the wave number range from 4000-400 cm^{-1}. The bands at 1635.71 and 3375.80 cm^{-1} represent the OH bend of the water and hydroxyl groups, respectively. The C=C bonds of the aromatic group can be confirmed by the band at 1600.44 cm^{-1}. The intensive band at 1384.23 cm^{-1} represents the N-O stretch due to the presence of nitrate. The absorption band at 494 cm^{-1} represents the O-Ce-O stretch which is in accordance with the previous studies[29]. In addition, the transmittance peaks obtained at 845 and 1062 cm^{-1} could be attributed to CO_3^{2-} bending vibration and C-O stretching vibration, respectively.

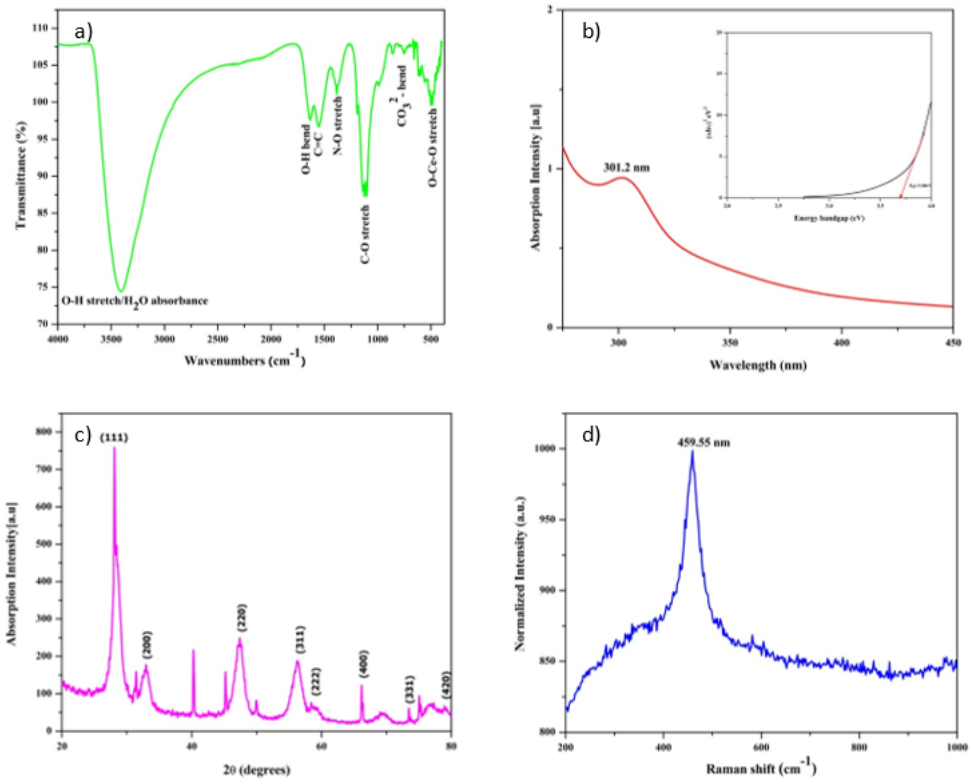

Fig 1. CeO_2 NPs Characterization (a) FTIR (b) UV-vis spectroscopy (inset, bandgap) (c) XRD pattern (d) Raman spectroscopy

Besides, the CeO_2 NPs formation can also portrayed from the UV-Visible absorbance spectrum (Figure 1 b). The UV-vis absorbance spectra were recorded for the nanoparticles against water as blank. A well-defined characteristic peak around

λ_{max} 301.2 nm was observed for the synthesized CeO_2 NPs, possibly due to an electron transition from the valence band to the conductance band. The absorption spectra obtained in the UV spectrometric analysis is very close to the band obtained for CeO_2 NPs, as reported in the previous study[30]. The optical bandgap energy was calculated using Tauc's relation.

$$\alpha h\upsilon = A\left(h\upsilon - E_g\right)^n \quad (2)$$

where hυ; photon energy, α; absorption coefficient ($\alpha = 4\pi k / \lambda$, k; absorption index or absorbance, λ; the wavelength in nanometer), E_g; energy band gap, A; constant, n = 1/2 for the allowed direct band gap. The exponent 'n' depends on the type of transition and it may have values 1/2, 2, 3/2 and 3 corresponding to the allowed direct, allowed indirect, forbidden direct and forbidden indirect transitions respectively. The energy bandgap value was determined by extrapolating the straight line (Figure 1 b, inset) and the value found to be around 3.68 eV. The band gap value was found to be lower than the CeO_2 NPs synthesized using Gloriosa superb leaf extract[31]. Further, the synthesized CeO_2 showed an increase in energy band gap compared to the bulk CeO_2 powder (Eg = 3.19 eV) which might be due to the quantum confinement in the system.

The crystalline structure of the synthesized CeO_2 NPs was studied using XRD, as shown in Figure 1 c. The sample was scanned from 10°-80° degrees with a scan rate of 2θ min^{-1}. The XRD spectra indicate the pure cubic fluorite structure and polycrystalline nature of the CeO_2 NPs. The high-intensity peaks observed at 28.55°, 33.08°, 47.48°, 56.33°, 59.09°, 69.40°, 76.70°, and 79.07° corresponds to the (111), (200), (220), (311), (222), (400), (331) and (420) crystal planes respectively. The crystal planes were in good accordance with JCPDS No 34-0394 and matched well with the previous XRD studies[16]. A characteristic impurity peak was observed, which may be due to an error while sample preparation, and this can be ignored as it is negligible impurity by considering the major phase of the cubic system. Further, the crystallite size and structural parameters such as d-spacing, lattice constant (Å), dislocation density (d) and microstrain (ε) estimated and represented in Table 2.

Table 2. CeO_2 NPs structural parameter data obtained from XRD analysis

CeO_2NPs	hkl planes		d-spacing		Lattice parameter(Å) a=b=c	Dislocationdensity (d)$\times 10^{15}$(l/m^2)	Microstrain (ε) $\times 10^{-3}$	Crystallite size (nm)
30 ml volume	(1,1,1)	(2,0,0)	3.123	2.706	5.409	1.94	2.38	22.67
	(2,2,0)	(3,1,1)	1.913	1.632				
	(2,2,2)	(4,0,0)	1.562	1.353				
	(3,3,1)		1.241					
	(4,2,0)		1.210					

Crystal System: Cubic, Space Group: Fm-3m (225)

Crystallite size was calculated using Debye's Scherrer equation.

$$D = \frac{K\lambda}{\beta cos\theta} \quad (3)$$

d-spacing was evaluated using the equation

$$n\lambda = 2d\ sin\theta \quad (4)$$

Where K is the shape factor, λ is the X-ray wavelength CuKα (1.5406 Å), β is the line broadening at half the maximum intensity (FWHM) in radians, and θ is the Bragg's angle, 'D' is the crystallite size. n is 1 (order of diffraction), d is interplanar spacing or Å. The average crystallite size was found to be 22.67 nm using *B. monnieri* leaf extract. The lattice parameter calculated from the reflection plane (111) for biosynthesized CeO_2 NPs by the below formula

$$a = d_{knl}\sqrt{h^2 + k^2 + l^2} \quad (5)$$

Where d is the spacing and hkl are the Miller indices. The calculated lattice parameters of biosynthesized CeO_2 NPs a= 0.5409 nm is small which indicates that the *B. monnieri* leaf extract might remain adhered on the surface of CeO_2 instead of comprising into the lattice of CeO_2 NPs. The micro strain (ε) of biosynthesized CeO_2 NPs was calculated by the formula

$$\varepsilon = \frac{\beta cos\theta}{4} \quad (6)$$

A dislocation density (δ) is a crystallographic defect in crystal structure. It was calculated using formula

$$\delta = \frac{1}{D^2}\ \text{lines}/\text{m}^2 \quad (7)$$

As depicted in Table 2, dislocation density is slightly higher than the pure CeO_2 as reported by the studies [32] which may be due to lesser oxygen vacancy present on the surface of CeO_2 NPs. However, the results of micro strain and dislocation density revealed the good lattice structure for CeO_2 NPs suggesting *B. monnieri* leaf extract can strongly influences the catalytic and electrochemical properties.

The presence of the cubic structure of the synthesized CeO_2 NPs by Raman spectroscopy is shown in Figure 1 d. The strong Raman band observed at 460 cm^{-1} (F_2g mode) is close to the characteristic Raman frequency as reported previously [33]. The obtained Raman peak confirms the presence of CeO_2 with cubic crystalline structure ascertained with the XRD result, which can be attributed to the symmetric vibrations of the Ce-O Raman active mode.

The morphological characterization was carried out to understand the size, shape, and surface morphology of CeO_2 NPs. SEM and EDAX profile of CeO_2 NPs is shown in Figure 2 a. The SEM image illustrates that the particles were uniform, tiny spherical, and the size ranges between 5-50nm. The EDAX spectra of synthesized NPs indicate the presence of cerium (77.07%) and oxygen (22.93%) in weight percentage. In contrast, the atomic % of elements Ce and O is 27.73% and 72.27%, respectively. Hence, the EDAX profile indicates the high purity of the synthesized CeO_2 NPs, which corresponds well with the XRD results.

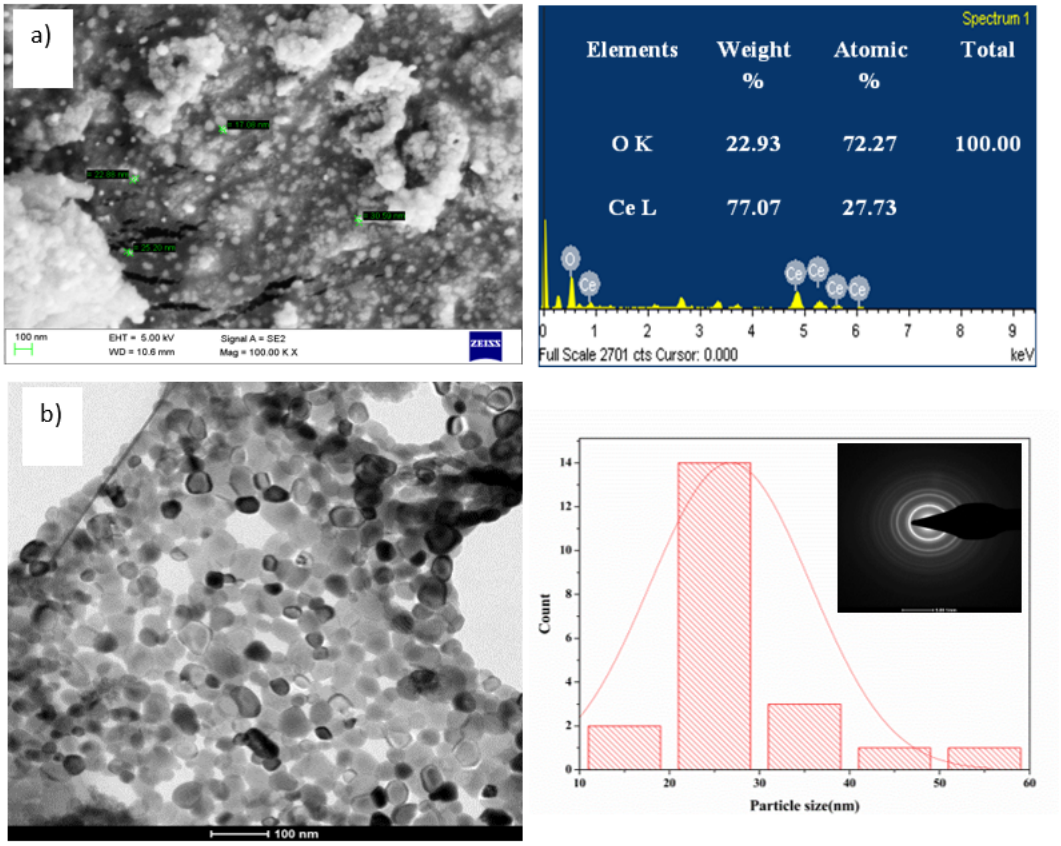

Fig 2. Morphological characterization of biosynthesized CeO_2NPs (a) SEM - EDAX analysis (b) HR-TEM analysis and size distribution histogram (inset, SAED pattern)

The detailed structural analysis of the CeO_2 NPs was characterized by HR-TEM and selected area electron diffraction (SAED). A low-magnification image of the NPs is depicted in Figure 2 b. Most of the particles are spherical, along with a few cubic particles with a mean size of 27 nm. The SAED pattern shows several weak Scherrer rings corresponding to the reflections of the cubic CeO_2 sample. The characterization results reveal that the synthesized CeO_2 NPs had a particle size in the nanoscale with high crystallinity.

Antioxidants are vital to the human body as it protects against oxidative damage by free radicals such as hydroxyl radicals, superoxide radicals, and singlet oxygen [34]. The hydroxyl [OH·] radical, generated by the Fenton reaction, contains a highly reactive oxygen center. It can bind the nucleotides in DNA and cause strand breakage that leads to mutagenesis, carcinogenesis, and cytotoxicity [14]. As cerium is a potent antioxidant, the effectiveness of synthesized CeO_2NPs was investigated by OH free

radical scavenging activity. The previous studies reported that biosynthesized CeO_2 NPs exhibited hydroxyl scavenging activity at higher concentration of 200 μg/mL and 500 μg/mL [14,35]. In our study, the biosynthesized CeO_2 NPs showed potent dose-dependent OH radical scavenging activity compared to Vitamin C at a lower concentration of 0.195-50μg/mL (Figure 3). This is possibly due to their explicit physicochemical properties and greater oxygen vacancy on CeO_2 NPs surface [36].

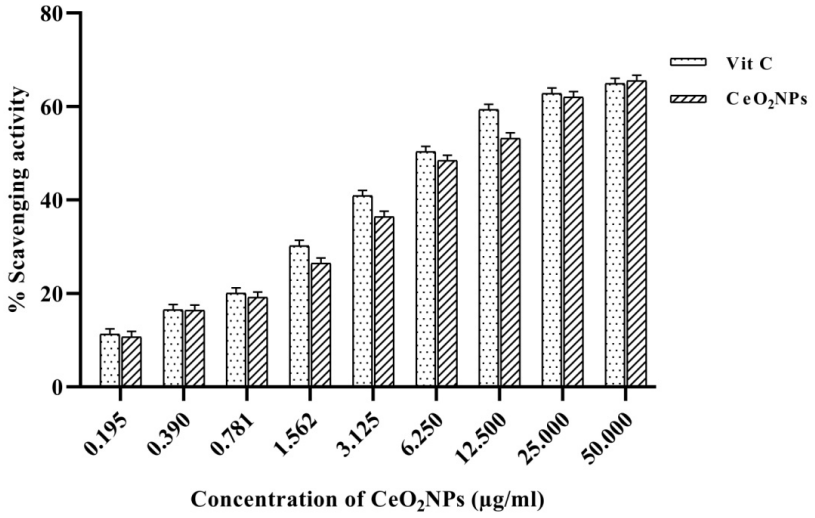

Fig 3. Dose dependent Hydroxyl radical scavenging activity of biosynthesized. CeO_2 NPs. Data represented as mean ± S.E (n=3)

4 Conclusion

CeO_2 NPs were successfully synthesized by an eco-friendly approach using the aqueous leaf extract of *B. monnieri* as a reducing agent leading to the reduction of metal nitrate into metal oxide. The biosynthesized CeO_2 NPs were characterized by techniques such as XRD, FTIR, UV-Vis, SEM and HR-TEM. XRD pattern elucidated the formation of pure cubic fluorite structure and polycrystalline nature. FTIR analysis confirms the presence of functional groups belonging to phytochemicals responsible for bioreduction during CeO_2 NPs formation. Besides, UV-Vis absorption at 301.2nm and Raman spectroscopy at 460 cm^{-1} revealed characteristic peaks that highly confirm the CeO_2 NPs formation. SEM and HR-TEM analysis revealed the formation of small spherical NPs and the EDAX profile confirms Ce-O elemental purity. The biosynthesized CeO_2 NPs exhibited better hydroxyl radical scavenging activity (65%) compared to vitamin C (60%). Thus, we can conclude that CeO_2 NPs show good antioxidant potential which may be utilized as a novel therapeutic agent in the treatment of oxidative stress-related disorders.

Acknowledgement

This work was supported by Bangalore University Research Promotion Board. We wish to thank Department of Microbiology and Biotechnology for providing infrastructural facilities.

References

1) Ding X, Lin K, Li Y, Dang M, Jiang L. Synthesis of Biocompatible Zinc Oxide (ZnO) Nanoparticles and Their Neuroprotective Effect of 6-OHDA Induced Neural Damage in SH-SY 5Y Cells. *Journal of Cluster Science*. 2020;31(6):1315–1328. Available from: https://doi.org/10.1007/s10876-019-01741-2.
2) Miri A, Darroudi M, Sarani M. Biosynthesis of cerium oxide nanoparticles and its cytotoxicity survey against colon cancer cell line. *Applied Organometallic Chemistry*. 2020;34(1). Available from: https://doi.org/10.1002/aoc.5308.
3) Mohammadzadeh V, Barani M, Amiri MS, Yazdi M, Hassanisaadi M, Rahdar A, et al. Applications of plant-based nanoparticles in nanomedicine: A review. 2022. Available from: https://doi.org/10.1016/j.scp.2022.100606.
4) Khan M, Mashwani Z, Ikram M, Raja NI, Mohamed AH, Ren G, et al. Efficacy of Green Cerium Oxide Nanoparticles for Potential Therapeutic Applications. *Circumstantial Insight on Mechanistic Aspects Nanomaterials*. 2022;12(12):2117. Available from: https://doi.org/10.3390/nano12122117.
5) Estevez AY, Ganesana M, Trentini JF, Olson JE, Li G, Boateng YO, et al. Antioxidant Enzyme-Mimetic Activity and Neuroprotective Effects of Cerium Oxide Nanoparticles Stabilized with Various Ratios of Citric Acid and EDTA. *Biomolecules*. 2019;9(10):562. Available from: https://doi.org/10.3390/biom9100562.

6) Hamidian K, Saberian MR, Miri A, Sharifi F, Sarani M. Doped and un-doped cerium oxide nanoparticles: Biosynthesis, characterization, and cytotoxic study. *Ceramics International*. 2021;47(10):13895–13902. Available from: https://doi.org/10.1016/j.ceramint.2021.01.256.
7) Adebayo OA, Akinloye O, Adaramoye OA. Cerium Oxide Nanoparticles Attenuate Oxidative Stress and Inflammation in the Liver of Diethylnitrosamine-Treated Mice. *Biological Trace Element Research*. 2020;193(1):214–225. Available from: https://doi.org/10.1007/s12011-019-01696-5.
8) Al-Snafi AE, Al-Sa'idy H, Hamid HK. The utilization of plant extracts/biomaterials for the green synthesis of nanoparticles, their biological activity, and mode of action. *Research Journal of Biology and Pharmacy*. 2022;06(01):17–46. Available from: https://doi.org/10.53022/oarjbp.2022.6.1.0063.
9) Chakraborty N, Banerjee J, Chakraborty P, Banerjee A, Chanda S, Ray KS, et al. Green synthesis of copper/copper oxide nanoparticles and their applications: a review. *Green Chemistry Letters and Reviews*. 2022;15(1):187–215. Available from: https://doi.org/10.1080/17518253.2022.2025916.
10) Jan H, Shah MA, Andleeb A, Faisal S, Khattak A, Rizwan M, et al. Plant-Based Synthesis of Zinc Oxide Nanoparticles (ZnO-NPs) Using Aqueous Leaf Extract of Aquilegia pubiflora: Their Antiproliferative Activity against HepG2 Cells Inducing Reactive Oxygen Species and Other In Vitro Properties. *Oxidative Medicine and Cellular Longevity*. 2021;2021:1–14. Available from: https://doi.org/10.1155/2021/4786227.
11) Jadoun S, Arif R, Jangid NK, Meena RK. Green synthesis of nanoparticles using plant extracts: a review. *Environmental Chemistry Letters*. 2021;19(1):355–374. Available from: https://doi.org/10.1007/s10311-020-01074-x.
12) Yazdi T, Ehsan M, Amiri MS, Akbari S, Sharifalhoseini M, Nourbakhsh F, et al. Green synthesis of silver nanoparticles using helichrysum graveolens for biomedical applications and waste water treatment. *BioNanoScience*. 2020;10(4):1121–1127. Available from: https://doi.org/10.1007/s12668-020-00794-2.
13) Nezhad AS, Es-Haghi A, Tabrizi MH. Green synthesis of cerium oxide nanoparticle using Origanum majorana L. leaf extract, its characterization and biological activities. *Applied Organometallic Chemistry*. 2020;34(2). Available from: https://doi.org/10.1002/aoc.5314.
14) Muthuvel A, Jothibas M, Manoharan C, Jayakumar SJ. Synthesis of CeO2-NPs by chemical and biological methods and their photocatalytic, antibacterial and in vitro antioxidant activity. *Research on Chemical Intermediates*. 2020;46(5):2705–2729. Available from: https://doi.org/10.1007/s11164-020-04115-w.
15) Ibrahim AM, Mohamed F, Al-Quraishy S, Abdel-Baki AAS, Abdel-Tawab H. Green synthesis of Cerium oxide / Moringa oleifera seed extract nano-composite and its molluscicidsal activities against biomophalaria alexanderina. *Journal of King Saud University - Science*. 2021;33(3):101368. Available from: https://doi.org/10.1016/j.jksus.2021.101368.
16) Magudieshwaran R, Ishii J, Raja KCN, Terashima C, Venkatachalam R, Fujishima A, et al. Green and chemical synthesized CeO2 nanoparticles for photocatalytic indoor air pollutant degradation. *Materials Letters*. 2019;239:40–44. Available from: https://doi.org/10.1016/j.matlet.2018.11.172.
17) Altaf M, Manoharadas S, Zeyad MT. Green synthesis of cerium oxide nanoparticles using Acorus calamus extract and their antibiofilm activity against bacterial pathogens. 2021. Available from: https://doi.org/10.53022/oarjbp.2022.6.1.0063.
18) Yang B, Dong Y, Wang F, Zhang Y. Nanoformulations to Enhance the Bioavailability and Physiological Functions of Polyphenols. *Molecules*. 2020;25(20):4613. Available from: https://doi.org/10.3390/molecules25204613.
19) Banerjee S, Anand U, Ghosh S, Ray D, Ray P, Nandy S, et al. Bacosides from <scp> Bacopa monnieri </scp> extract: An overview of the effects on neurological disorders. *Phytotherapy Research*. 2021;35(10):5668–5679. Available from: https://doi.org/10.1002/ptr.7203.
20) Brimson JM, Brimson SM, Prasanth MI, Thitilertdecha P, Malar DS, Tencomnao T. The effectiveness of Bacopa monnieri (Linn.) Wettst. as a nootropic, neuroprotective, or antidepressant supplement: analysis of the available clinical data. *Scientific Reports*. 2021;11(1):1–11. Available from: https://doi.org/10.1038/s41598-020-80045-2.
21) Yulizar Y, Kusrini E, Apriandanu DOB, Nurdini N. Datura metel L. Leaves extract mediated CeO2 nanoparticles: Synthesis, characterizations, and degradation activity of DPPH radical. *Surfaces and Interfaces*. 2020;19:100437. Available from: https://doi.org/10.1016/j.surfin.2020.100437.
22) Navada MK, Karnikkar NG, D'souza JN, Kouser SN, Aroor G, Kudva J, et al. Biosynthesis of phyto functionalized cerium oxide nanoparticles mediated from Scoparia dulsis L. for appraisal of anti-cancer potential against adenocarcinomic lung cancer cells and paracetamol sensing potentiality. *Environmental Science and Pollution Research*. 2022;30(7):18901–18920. Available from: https://doi.org/10.1007/s11356-022-23500-z.
23) Ganeshkar MP, Goder PH, Mirjankar MR, Gaddigal AT, Shivappa P, Kamanavalli CM. Characterization and screening of anticancer properties of cerium oxide nanoparticles synthesized using Averrhoa carambola plant extract. *Inorganic and Nano-Metal Chemistry*. 2022;p. 1–14. Available from: https://doi.org/10.1080/24701556.2022.2077374.
24) Kahsay MH. Synthesis and characterization of ZnO nanoparticles using aqueous extract of Becium grandiflorum for antimicrobial activity and adsorption of methylene blue. *Applied Water Science*. 2021;11(2):1–12. Available from: https://doi.org/10.1007/s13201-021-01373-w.
25) Jawhari FZ, Moussaoui AEL, Bourhia M, Imtara H, Saghrouchni H, Ammor K, et al. Anacyclus pyrethrum var. pyrethrum (L.) and Anacyclus pyrethrum var. depressus (Ball) Maire: Correlation between Total Phenolic and Flavonoid Contents with Antioxidant and Antimicrobial Activities of Chemically Characterized Extracts. *Plants*. 2021;10(1):149. Available from: https://doi.org/10.3390/plants10010149.
26) Diab TA, Donia T, Saad-Allah KM. Characterization, antioxidant, and cytotoxic effects of some Egyptian wild plant extracts. *Beni-Suef University Journal of Basic and Applied Sciences*. 2021;10(1):1–13. Available from: https://doi.org/10.1186/s43088-021-00103-0.
27) Lakshmeesha TR, Kalagatur NK, Mudili V, Mohan CD, Rangappa S, Prasad BD, et al. Biofabrication of Zinc Oxide Nanoparticles With Syzygium aromaticum Flower Buds Extract and Finding Its Novel Application in Controlling the Growth and Mycotoxins of Fusarium graminearum. *Frontiers in Microbiology*. 2019;10:1244. Available from: https://doi.org/10.3389/fmicb.2019.01244.
28) Adefegha SA, Olasehinde TA, Oboh G. Essential Oil Composition, Antioxidant, Antidiabetic and Antihypertensive Properties of Two Afromomum Species. *Journal of Oleo Science*. 2017;66(1):51–63. Available from: https://doi.org/10.5650/jos.ess16029.
29) Naz S, Kazmi STB, Zia M. CeO ₂ nanoparticles synthesized through green chemistry are biocompatible: In vitro and in vivo assessment. *Journal of Biochemical and Molecular Toxicology*. 2019;33(5):e22291. Available from: https://doi.org/10.1002/jbt.22291.
30) Anastasia Mikhailovna Korotkova, Borisovna PO, Aleksandrovna GI, Bagdasarovna KD, Vladimirovich BD, Vladimirovich KD, et al. "Green" Synthesis of Cerium Oxide Particles in Water Extracts Petroselinum crispum. *Current Nanomaterials*. 2019;4(3):176–190. Available from: https://doi.org/10.2174/2405461504666190911155421.
31) Arumugam A, Karthikeyan C, Hameed ASH, Gopinath K, Gowri S, Karthika V. Synthesis of cerium oxide nanoparticles using Gloriosa superba L. leaf extract and their structural, optical and antibacterial properties. *Materials Science and Engineering: C*. 2015;49:408–415. Available from: https://doi.org/10.1016/j.msec.2015.01.042.
32) Hemalatha KS, Rukmani K. Synthesis, characterization and optical properties of polyvinyl alcohol–cerium oxide nanocomposite films. *RSC Advances*. 2016;6(78):74354–74366. Available from: https://doi.org/10.1039/c6ra11126b.
33) Kumar S, Ahmed F, Shaalan NM, Saber O. Biosynthesis of CeO2 Nanoparticles Using Egg White and Their Antibacterial and Antibiofilm Properties on Clinical Isolates. *Crystals*. 2021;11(6):584. Available from: https://doi.org/10.3390/cryst11060584.

34) Pardhiya S, Priyadarshini E, Rajamani P. In vitro antioxidant activity of synthesized BSA conjugated manganese dioxide nanoparticles. *SN Applied Sciences*. 2020;2(9):1–12. Available from: https://doi.org/10.1007/s42452-020-03407-5.
35) Rajan AR, Vilas V, Rajan AR, John A, Philip D. Synthesis of CeO2 nanostructures with its exceptional biological and chemocatalytic activities: a comparative study. *Bulletin of Materials Science*. 2021;44(1):1–10. Available from: https://doi.org/10.1007/s12034-020-02315-z.
36) Yadav N, Singh S. Polyoxometalate-Mediated Vacancy-Engineered Cerium Oxide Nanoparticles Exhibiting Controlled Biological Enzyme-Mimicking Activities. *Inorganic Chemistry*. 2021;60(10):7475–7489. Available from: https://doi.org/10.1021/acs.inorgchem.1c00766.